The Metal-rich Phosphide $Ce_4Ir_{13.55}P_9$

Ulrike Pfannenschmidt, Ute Ch. Rodewald, and Rainer Pöttgen

Institut für Anorganische und Analytische Chemie, Universität Münster, Corrensstraße 30, 48149 Münster, Germany

Reprint requests to R. Pöttgen. E-mail: pottgen@uni-muenster.de

Z. Naturforsch. **2011**, *66b,* 7 – 13; received October 1, 2010

Needle-shaped crystals of the metal-rich phosphide $Ce_4Ir_{13.55}P_9$ were synthesized from the elements in a lead flux (starting composition 1 : 2 : 2 : 60) at 1370 K followed by slow cooling. $Ce_4Ir_{13.55}P_9$ crystallizes with a new orthorhombic structure type: *Pnma*, $a = 1269.1(2)$, $b = 399.1(1)$, $c = 3349.9(7)$ pm, $wR2 = 0.0722$, 2025 F^2 values and 139 variables. Two of the 14 crystallographic iridium sites show small defects. All phosphorus atoms have slightly distorted tricapped trigonal prismatic metal coordination by cerium and iridium. The iridium and phosphorus atoms build up a three-dimensional $[Ir_{13.55}P_9]^{\delta-}$ polyanion in which the cerium atoms fill distorted hexagonal cavities. Within the polyanion the phosphide anions are isolated, and one additionally observes a broad range of Ir–Ir bonding (Ir–Ir distances 278 – 298 pm). From a geometrical point of view the $Ce_4Ir_{13.55}P_9$ structure can be considered as an intergrowth structure of distorted $ThCr_2Si_2$- and SrPtSb-related slabs.

Key words: Phosphide, Cerium, Crystal Chemistry

Introduction

Metal-rich phosphides with a metal : phosphorus ratio of exactly or nearly 2 : 1 have intensively been investigated in the last thirty years with respect to their crystal structures and physical properties. The basic data have been summarized in review articles [1 – 5]. Although many of these phosphide structures are rather complex, they have a common structural motif, *i. e.* the phosphorus atoms show tricapped trigonal-prismatic metal coordination. Most investigations in this field have been carried out in the systems rare earth (*RE*)-transition metal (*T*)-phosphorus, and many representatives are known for compositions *RE* : *T* : P of 1 : 1 : 1, 2 : 12 : 7, 6 : 20 : 13, or 5 : 19 : 12. Geometrically, these and related complex structures can easily be distinguished by the connectivity pattern of the phosphorus-centered trigonal prisms. Various examples are given in [6 – 9].

Well shaped single crystals of the metal-rich $RE_xT_yP_z$ phosphides can be grown in metal fluxes [10], *e. g.* tin, lead, or bismuth. So far, the *RE*-*T*-P systems have mostly been studied with the 3*d* metals Fe, Co, Ni, and Cu [1]. Besides the high price of the noble metals, especially the lower reactivity of the 4*d* and 5*d* transition metals has hampered such investigations. We have recently picked up this topic and grew single crystals of $Lu_3Ir_7P_5$ [11] and $Sm_{15}Ir_{33}P_{26}$ [12] in bismuth and lead fluxes. Although these structures are quite complex with a large unit cell content (Pearson symbols oS120 and mC148, respectively), they can geometrically be described as intergrowth structures of simpler structure types, *i. e.* $ThCr_2Si_2$ (tI10), SrPtSb (hP3), $CeMg_2Si_2$ (tP5), and TiNiSi (oP12). This seems to be a general structural principle of the metal-rich $RE_xIr_yP_z$ phosphides, since also the structures of $La_6Ir_{20}P_{13}$, $Ce_5Ir_{19}P_{12}$, $La_6Ir_{32}P_{17}$, $Gd_7Ir_{17}P_{12}$, and $Ce_{13}Ir_{35}P_{24}$ [13] can be described in this way. Herein we report on the lead flux growth of single crystals of $Ce_4Ir_{13.55}P_9$, a new complex phosphide with distorted $ThCr_2Si_2$- and SrPtSb-related slabs.

Experimental Section

Synthesis

Needle-shaped single crystals of $Ce_4Ir_{13.55}P_9$ were obtained from a lead flux. Starting materials were cerium filings (Heraeus, 99.9 %), iridium powder (Heraeus, > 99.9 %), red phosphorus (Hoechst, Knapsack, ultrapure), and lead granules (ABCR GmbH, > 99.99 %). A mixture of the molar ratio of 1 : 2 : 2 : 60 (Ce : Ir : P : Pb) was placed in an alumina crucible, which was sealed in an evacuated silica tube. The ampoule was positioned in a muffle furnace, heated to 770 K at a rate of 50 K h^{-1} and kept at that temperature for a period

Table 1. Crystal data and structure refinement for $Ce_4Ir_{13.55}P_9$, space group *Pnma*, $Z = 4$.

Refined composition	$Ce_4Ir_{13.55}P_9$
Formula weight, g mol^{-1}	3438.95
Crystal size, μm^3	$10 \times 10 \times 80$
Unit cell dimensions (Guinier data)	
a, pm	1269.1(2)
b, pm	399.1(1)
c, pm	3349.9(7)
Cell volume, nm^3	1.6967
Calculated density, g cm^{-3}	13.48
$F(000)$, e	5640
Absorption coefficient, mm^{-1}	117.0
Transm. ratio, max / min	0.783 / 0.081
Detector distance, mm	120
Exposure time, min	12
ω range; increment, deg	0 – 180, 0.7
Integr. param. A, B, EMS	12.0, 2.4, 0.11
θ range for data collection, deg	1.7 – 26.8
Range in *hkl*	± 16, ± 5, ± 41
Total no. reflections	12234
Independent reflections / $R_{\rm int}$	2025 / 0.1780
Reflections with $I \geq 2\sigma(I)$ / R_σ	1062 / 0.1292
Data / ref. parameters	2025 / 139
$R1/wR2$ for $I \geq 2\sigma(I)$	0.0370 / 0.0585
$R1/wR2$ for all data	0.0996 / 0.0722
Goodness-of-fit on F^2	0.684
Extinction coefficient	0.000010(3)
Largest diff. peak / hole, e Å^{-3}	3.16 / −2.79

of 24 h, and then the temperature was raised to 1370 K at the same rate. After keeping that temperature for 100 h the ampoule was slowly cooled to r. t. at a rate of 2 K h^{-1}. The excess lead flux was dissolved by a 1 : 1 molar mixture of H_2O_2 (Acros 35 %) and glacial acetic acid (VWR International, > 99.8 %). The resulting sample was washed with demineralized water. The reaction product consists of intergrown aggregates of needle-shaped crystals of $Ce_4Ir_{13.55}P_9$ besides platelets of the by-product $CeIr_2P_2$. Both crystal types have metallic luster. $Ce_4Ir_{13.55}P_9$ is stable in air.

EDX data

The single crystal investigated on the diffractometer was studied by EDX using a Zeiss EVO MA10 scanning electron microscope with CeO_2, Ir and GaP as standards for the semi-quantitative measurements. The analyses indicated Ce, Ir and P as main components. Due to the significant overlap of the phosphorus *K* (2.1013 keV) and iridium *M* (1.977 keV) lines, a quantitative analysis was not possible. No other impurity elements (especially no lead incorporation from the flux) were observed.

X-Ray diffraction

The flux-grown $Ce_4Ir_{13.55}P_9$ sample (selected needle-shaped crystals) was characterized by X-ray powder diffraction on a Guinier camera (equipped with an image plate system Fujifilm, BAS-1800) using Cu$K_{\alpha 1}$ radiation and α-quartz (a = 491.30, c = 540.46 pm) as an internal standard. The orthorhombic lattice parameters (Table 1) were deduced from a least-squares refinement of the powder data. To ensure correct indexing, the experimental pattern was compared to a calculated one [14] using the positional parameters obtained from the structure refinement.

Needle-shaped crystal fragments of $Ce_4Ir_{13.55}P_9$ were separated from the agglomerated flux-grown sample by mechanical fragmentation. The needles were glued to quartz fibres using beeswax and were characterized by Laue photographs on a Buerger camera (white molybdenum radiation, image plate technique, Fujifilm, BAS-1800) in order to check their suitability for an intensity data collection. The data set was collected at r. t. by use of an IPDS II diffractometer (graphite-monochromatized MoK_α radiation; oscillation mode). A numerical absorption correction was applied to the data set. All relevant crystallographic data and details of the data collection and evaluation are listed in Table 1.

Structure refinement

Careful analyses of the diffractometer data set revealed a primitive orthorhombic lattice, and the systematic extinctions were compatible with the centrosymmetric space group *Pnma*. The starting atomic parameters were then determined *via* Direct Methods with SHELXS-97 [15], and the structure was refined using SHELXL-97 [16] (full-matrix least-squares on F^2) with anisotropic atomic displacement parameters for all metal sites. In view of the enhanced standard deviations of the isotropic displacement parameters of the phosphorus sites, an anisotropic refinement was not possible. As a check for the correct composition, the occupancy parameters were refined in a separate series of least-squares cycles. Similar to the recently refined structures of $Lu_3Ir_{6.97}P_5$ [11] and $Sm_{15}Ir_{32.50}P_{26}$ [12], two iridium sites of the present phosphide also showed small defects. The occupancy parameters of Ir9 and Ir13 were then refined as least-squares variables in the final refinement cycles, leading to the composition $Ce_4Ir_{13.55}P_9$ for the investigated crystal. All other sites were fully occupied within two standard deviations. The final difference Fourier synthesis was flat (Table 1). The positional parameters and interatomic distances are listed in Tables 2 and 3.

Further details of the crystal structure investigation may be obtained from Fachinformationszentrum Karlsruhe, 76344 Eggenstein-Leopoldshafen, Germany (fax: +49-7247-808-666; e-mail: crysdata@fiz-karlsruhe.de, http://www.fiz-informationsdienste.de/en/DB/icsd/depot_anforderung.html) on quoting the deposition number CSD-422192.

Discussion

The phosphide $Ce_4Ir_{13.55}P_9$ crystallizes with a new orthorhombic structure type. The unit cell contains

Atom	x	z	U_{11}	U_{22}	U_{33}	U_{13}	U_{eq} / U_{iso}
Ce1	0.2030(2)	0.47617(8)	101(11)	66(14)	121(14)	−20(10)	96(6)
Ce2	0.2021(2)	0.35358(8)	71(12)	27(15)	157(13)	30(10)	85(6)
Ce3	0.2067(2)	0.69566(8)	79(11)	30(15)	104(12)	−18(9)	71(6)
Ce4	0.4779(2)	0.41912(8)	47(9)	54(11)	95(10)	0(9)	65(4)
Ir1	0.4958(1)	0.97083(6)	93(8)	77(9)	94(7)	3(7)	88(3)
Ir2	0.7056(1)	0.58301(6)	66(7)	101(9)	112(7)	6(7)	93(4)
Ir3	0.2123(1)	0.04303(5)	92(8)	60(11)	128(8)	−2(7)	93(4)
Ir4	0.4292(2)	0.64858(5)	87(8)	65(10)	136(8)	1(7)	96(4)
Ir5	0.0074(1)	0.41324(6)	103(7)	55(8)	126(7)	−12(7)	94(3)
Ir6	0.1955(1)	0.79125(6)	91(8)	71(10)	113(8)	11(7)	92(4)
Ir7	0.2190(1)	0.12832(5)	59(8)	73(10)	121(8)	9(7)	84(4)
Ir8	0.4295(2)	0.51556(5)	87(8)	66(10)	127(7)	2(6)	93(4)
Ir9[a]	0.1663(2)	0.58583(9)	112(12)	113(13)	201(13)	5(11)	142(8)
Ir10	0.4375(1)	0.32201(5)	66(7)	59(10)	135(8)	−10(7)	87(4)
Ir11	0.4837(1)	0.20500(5)	91(7)	59(9)	109(8)	7(7)	86(4)
Ir12	0.1780(1)	0.25397(5)	75(8)	77(11)	116(8)	14(7)	89(4)
Ir13[a]	0.4762(2)	0.73451(7)	151(14)	89(14)	138(13)	39(9)	126(9)
Ir14	0.4922(2)	0.85443(5)	101(8)	41(10)	135(8)	−2(7)	92(4)
P1	0.6179(9)	0.5208(3)					101(25)
P2	0.3872(8)	0.9141(4)					95(21)
P3	0.3925(8)	0.0321(4)					101(23)
P4	0.3450(8)	0.5829(4)					139(22)
P5	0.1150(9)	0.8571(3)					84(23)
P6	0.3639(9)	0.2570(3)					88(23)
P7	0.3876(9)	0.7940(3)					94(23)
P8	0.1187(9)	0.1876(3)					87(22)
P9	0.3940(9)	0.1424(3)					85(23)

Table 2. Atomic coordinates and anisotropic displacement parameters (pm^2) for $Ce_4Ir_{13.55}P_9$. U_{eq} is defined as one third of the trace of the orthogonalized U_{ij} tensor. The anisotropic displacement factor exponent takes the form: $-2\pi^2[(ha*)2U_{11} + \ldots + 2hka*b*U_{12}]$. $U_{12} = U_{23} = 0$. The phosphorus atoms have been refined isotropically. All atoms lie on Wyckoff positions 4*c* (*x*, 1/4, *z*).

[a] The Ir9 and Ir13 sites are only occupied by 77.1(9) % and 77.6(10) %, respectively.

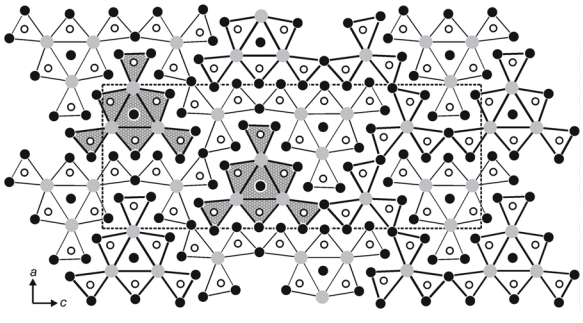

Fig. 1. Projection of the $Ce_4Ir_{13.55}P_9$ structure along the short unit cell axis. All atoms lie on mirror planes at y = 1/4 (thin lines) and y = 3/4 (thick lines). Cerium, iridium, and phosphorus atoms are drawn as medium grey, filled, and open circles, respectively. The trigonal prisms around the phosphorus atoms are emphasized.

four formula units, *i. e.* 108 atoms. All phosphorus atoms in $Ce_4Ir_{13.55}P_9$ are *isolated* from each other. They all have a slightly distorted tricapped trigonal-prismatic metal coordination, as typically observed in metal-rich phosphides. These trigonal prisms are condensed *via* common edges within the crystallographic *xz* plane and common triangular faces along *y*, leading to the structural motif presented in Fig. 1. Prisms drawn with thin and thick lines are shifted by half the translation period *y*. Although this structural description is a purely geometrical one, it is very efficient to discriminate the different structure types of metal-rich phosphides. Depending on the $RE:T$ ratio, the trigonal prisms show different connectivity patterns. For $Ce_4Ir_{13.55}P_9$, the central propellar-like motif of six condensed prisms is similar to the structures of $U_6Rh_{20}P_{13}$ [17] and $Hf_2Co_4P_3$ [18] (Fig. 2). For further connectivity patterns we refer to [1, 6 – 9].

Another possibility to describe such complex structures is the concept of intergrowth structures [19]. As emphasized in Fig. 3, the complex structure of $Ce_4Ir_{13.55}P_9$ can easily be described as an intergrowth variant of slightly distorted $ThCr_2Si_2$- and SrPtSb (ordered AlB_2)-related slabs. While $CeIr_2P_2$ [20] crystallizes with the $CaBe_2Ge_2$ type (space group $P4/nmm$) with an $[Ir_2P_2]$ network closely related to $ThCr_2Si_2$, CeIrP [21] adopts the LaPtSi type (space group $I4_1md$), where the phosphorus and iridium atoms also have distorted trigonal-prismatic coordination.

At the left-hand side of Fig. 3 we have emphasized the $[Ir_{13.55}P_9]$ network of $Ce_4Ir_{13.55}P_9$. The 14 crystallographically independent iridium atoms within the $[Ir_{13.55}P_9]$ network have between 2 and 5 phosphorus atoms at Ir–P distances ranging from 227 to 286 pm.

Table 3. Interatomic distances (pm) in $Ce_4Ir_{13.55}P_9$. All distances within the first coordination spheres are listed. Standard deviations are given in parentheses.

Ce1:	2	P3	299.3(8)	Ir2:	1	P2	231(1)	Ir9:	1	P4	227(1)	P2:	1	Ir2	231(1)
	2	P1	302.6(8)		1	P5	231(1)		2	P3	278.9(9)		1	Ir1	235(1)
	2	Ir2	304.2(3)		1	P1	236(1)		2	Ir7	285.1(2)		1	Ir14	240(1)
	2	P2	310(1)		2	Ce1	304.3(3)		2	P9	285.7(8)		2	Ir5	240.3(6)
	1	Ir8	316.3(3)		2	Ce4	306.8(2)		1	Ir1	287.8(3)		2	Ce2	306(1)
	1	Ir1	317.3(3)		2	Ce2	314.1(3)		2	Ir3	290.1(2)		2	Ce1	310(1)
	2	Ir3	318.6(3)	Ir3:	1	P3	232(1)		2	Ir5	297.3(2)	P3:	1	Ir3	232(1)
	2	Ir1	322.2(2)		1	P1	245(1)		1	Ir14	298.0(3)		1	Ir5	234(1)
	1	Ir5	325.7(3)		2	P4	250.9(7)	Ir10:	1	P8	232(1)		1	Ir1	244(1)
Ce2:	2	P7	304.4(9)		2	Ir8	284.0(2)		1	P6	237(1)		2	Ir1	245.0(6)
	2	P2	306(1)		1	Ir7	285.8(3)		2	P5	241.0(6)		2	Ir9	278.9(9)
	2	P5	306.3(9)		2	Ir9	290.1(2)		2	Ir4	279.6(2)		2	Ce1	299.3(9)
	2	Ir2	314.1(3)		2	Ce1	318.6(3)		2	Ir6	280.9(2)	P4:	1	Ir9	227(1)
	2	Ir6	316.7(3)		1	Ce4	323.4(3)		2	Ir13	296.1(2)		1	Ir4	245(1)
	1	Ir10	316.9(3)	Ir4:	1	P5	237(1)		1	Ce2	316.9(3)		1	Ir8	250(1)
	2	Ir14	317.3(3)		1	P4	245(1)		1	Ce4	329.3(3)		2	Ir3	250.9(7)
	1	Ir5	317.8(3)		2	P8	246.2(7)	Ir11:	1	P6	231(1)		2	Ir7	263.7(8)
	1	Ir12	335.1(3)		2	Ir10	279.6(2)		1	P9	239(1)		2	Ce4	300.6(8)
	1	Ir11	339.6(3)		2	Ir7	282.4(2)		2	P7	257.9(7)	P5:	1	Ir2	231(1)
Ce3:	2	P9	296.6(9)		1	Ir13	294.0(3)		1	Ir12	282.3(3)		1	Ir4	237(1)
	2	P8	299.4(8)		1	Ce3	323.4(3)		2	Ir14	283.5(2)		2	Ir10	241.0(6)
	2	P6	300.0(9)		2	Ce4	324.3(3)		2	Ir13	288.9(2)		1	Ir6	243(1)
	2	Ir11	315.0(3)	Ir5:	1	P3	234(1)		2	Ce3	315.0(3)		2	Ce2	306.3(9)
	2	Ir12	315.3(3)		1	P9	235(1)		1	Ce2	339.6(3)		2	Ce4	311.2(9)
	2	Ir7	315.6(3)		2	P2	240.3(6)	Ir12:	1	P8	235(1)	P6:	1	Ir11	231(1)
	1	Ir14	319.8(3)		2	Ir1	277.6(2)		1	P6	236(1)		1	Ir12	236(1)
	1	Ir6	320.5(3)		2	Ir14	280.4(2)		2	P7	254.4(7)		1	Ir10	237(1)
	1	Ir4	323.4(3)		2	Ir9	297.3(2)		1	Ir11	282.3(3)		2	Ir6	242.2(6)
Ce4:	2	P4	300.6(8)		1	Ce2	317.8(3)		2	Ir6	285.0(2)		2	Ir13	286.1(8)
	2	Ir2	306.8(2)		1	Ce1	325.7(3)		2	Ir13	286.9(2)		2	Ce3	300.1(9)
	2	P1	308.4(8)	Ir6:	2	P6	242.2(6)		2	Ce3	315.3(3)	P7:	1	Ir13	229(1)
	2	P5	311.2(9)		1	P5	243(1)		1	Ce2	335.1(3)		1	Ir14	242(1)
	2	Ir8	318.6(3)		1	P7	244(1)	Ir13:	1	P7	229(1)		1	Ir6	244(1)
	1	Ir3	323.4(3)		2	Ir10	280.9(2)		2	P8	281.1(8)		2	Ir12	254.4(7)
	2	Ir4	324.3(3)		2	Ir12	285.0(2)		2	P6	286.1(8)		2	Ir11	257.9(7)
	1	Ir8	328.9(3)		1	Ir13	291.4(3)		2	Ir12	286.9(2)		2	Ce2	304.4(9)
	1	Ir10	329.3(3)		2	Ce2	316.7(3)		2	Ir11	288.9(2)	P8:	1	Ir10	232(1)
	1	Ir7	344.8(3)		1	Ce3	320.5(3)		1	Ir6	291.4(3)		1	Ir12	235(1)
Ir1:	1	P2	235(1)	Ir7:	1	P9	227(1)		1	Ir4	294.0(3)		1	Ir7	236(1)
	1	P3	244(1)		1	P8	236(1)		2	Ir10	296.1(2)		2	Ir4	246.2(7)
	2	P3	245.0(6)		2	P4	263.7(8)	Ir14:	1	P2	240(1)		2	Ir13	281.0(8)
	2	Ir5	277.6(2)		2	Ir4	282.4(2)		1	P7	242(1)		2	Ce3	299.4(8)
	2	Ir1	279.5(3)		2	Ir9	285.1(2)		2	P9	246.5(7)	P9:	1	Ir7	227(1)
	1	Ir9	287.8(3)		1	Ir3	285.8(3)		2	Ir5	280.4(2)		1	Ir5	235(1)
	1	Ce1	317.3(3)		2	Ce3	315.6(3)		2	Ir11	283.5(2)		1	Ir11	239(1)
	2	Ce1	322.2(2)		1	Ce4	344.8(3)		1	Ir9	298.1(3)		2	Ir14	246.5(7)
				Ir8:	1	P1	240(1)		2	Ce2	317.3(3)		1	Ir9	285.6(8)
					2	P1	241.5(6)		1	Ce3	319.7(3)		2	Ce3	296.6(9)
					1	P4	250(1)	P1:	1	Ir2	236(1)				
					2	Ir3	284.0(2)		1	Ir8	240(1)				
					2	Ir8	287.6(3)		2	Ir8	241.4(6)				
					1	Ce1	316.3(3)		1	Ir3	245(1)				
					2	Ce4	318.6(3)		2	Ce1	302.6(8)				
					1	Ce4	328.9(3)		2	Ce4	308.4(8)				
									1	Ce4	384(1)				

The shorter ones compare well with the sum of the covalent radii [22] of 236 pm for Ir + P, and we can assume substantial Ir-P bonding within the polyanion. A comparable range of Ir–P distances occurs in

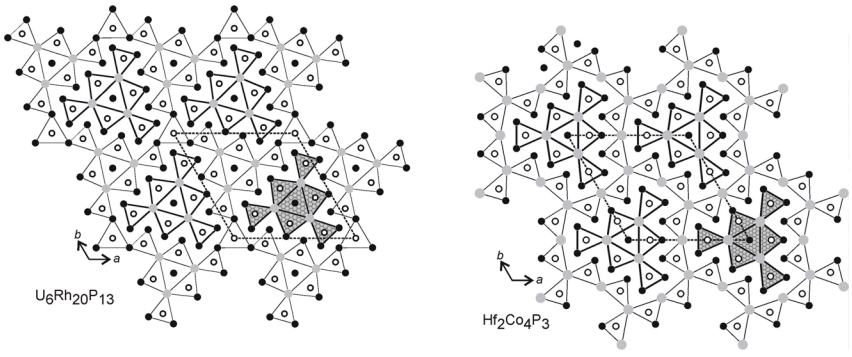

Fig. 2. Projection of the $U_6Rh_{20}P_{13}$ [17] and $Hf_2Co_4P_3$ [18] structures along the short unit cell axis. Uranium (hafnium), transition metal, and phosphorus atoms are drawn as medium grey, filled, and open circles, respectively. The trigonal prisms around the phosphorus atoms are emphasized. Prisms drawn with thin and thick lines are shifted by half a translation period.

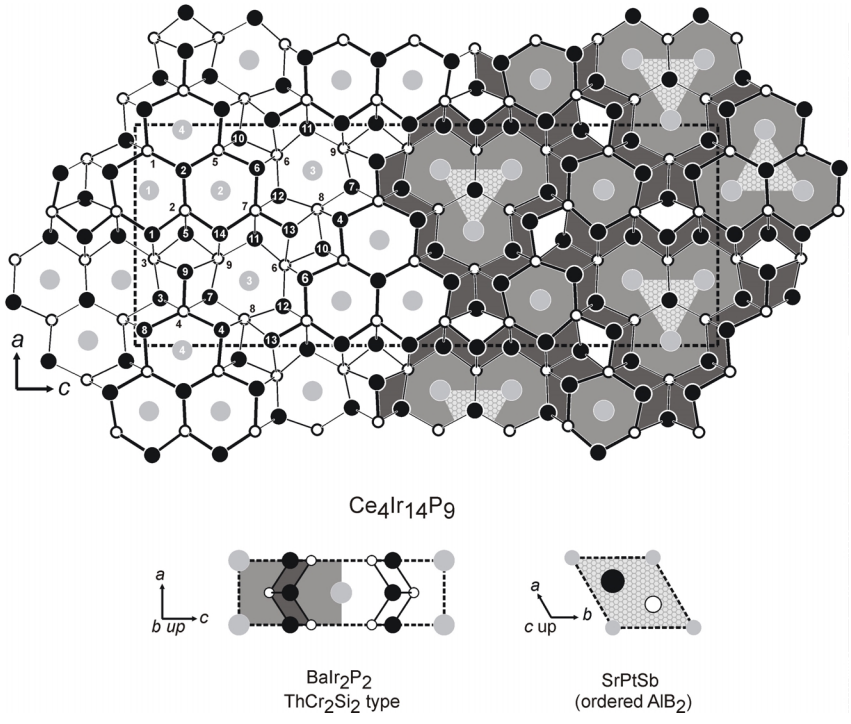

Fig. 3. Projection of the $Ce_4Ir_{13.55}P_9$ structure onto the *xz* plane. All atoms lie on mirror planes at $y = 1/4$ (thin lines) and $y = 3/4$ (thick lines). Cerium, iridium, and phosphorus atoms are drawn as medium grey, filled, and open circles, respectively. The three-dimensional $[Ir_{13.55}P_9]$ network is emphasized, and atom designations are given in one part of the unit cell. The right-hand part of the drawing highlights the intergrowth character of $ThCr_2Si_2$- ($BaIr_2P_2$) and SrPtSb- (ordered AlB_2) related slabs. For details see text.

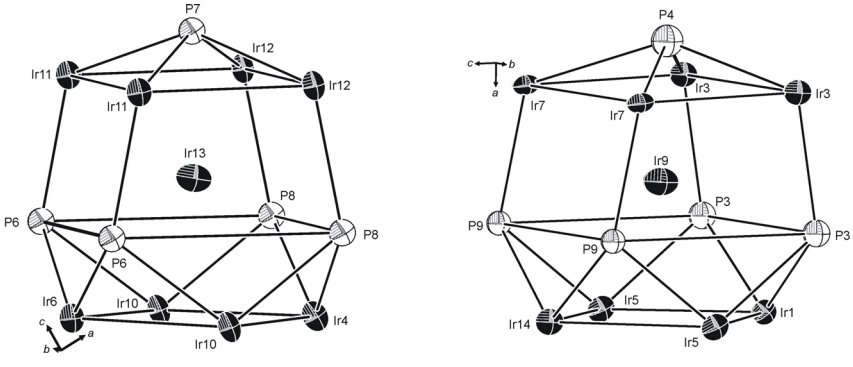

Fig. 4. Coordination of the Ir13 and Ir9 atoms in the $Ce_4Ir_{13.55}P_9$ structure. Atom labels are given. The displacement ellipsoids are drawn at the 80 % probability limit. For details see text.

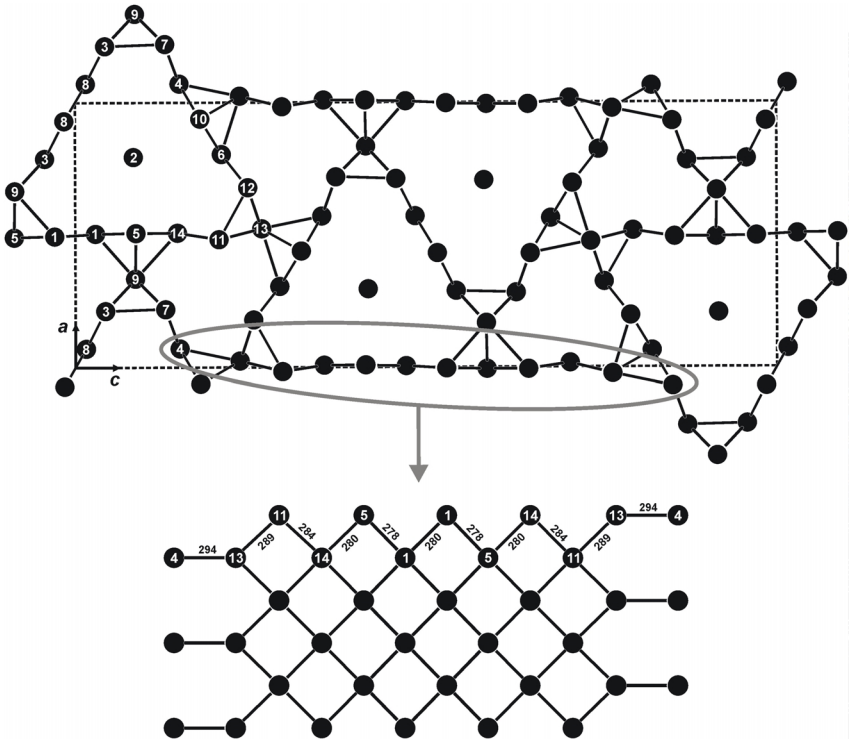

Fig. 5. Top: The iridium substructure of $Ce_4Ir_{13.55}P_9$ as a projection onto the *xz* plane. Bottom: Cutout of the iridium substructure with a view along *x* (*y* up). In all of these subunits, slightly distorted squares extend in the *y* direction. Atom designations and relevant interatomic distances are given.

$Lu_3Ir_{6.97}P_5$ [11] and $Sm_{15}Ir_{32.50}P_{26}$ [12] as well as in several alkaline earth-iridium-phosphides [21, 23, 24].

The cerium atoms fill distorted hexagonal cages within the $[Ir_{13.55}P_9]$ network (Fig. 3). The four crystallographically independent cerium atoms all bond to the polyanion *via* Ce-P contacts. The various Ce–P distances range from 297 to 311 pm, slightly longer than in NaCl-type CeP (284 pm) [25]. The shortest Ce–Ce distance of 399 pm corresponds to the *b* lattice parameter. Thus, all Ce–Ce distances are longer than in *fcc* cerium (365 pm) [26] and well above the Hill limit for *f*-electron localization [27]. The cerium atoms transfer part of their valence electrons to enable the covalent Ir-P bonding within the polyanion. In view of the long distances and the charge transfer we can safely rule out Ce–Ce bonding in $Ce_4Ir_{13.55}P_9$.

As a consequence of the high iridium content we observe a broad range of Ir–Ir distances of 278 – 298 pm, slightly longer than in *fcc* iridium (272 pm) [26]. Within the $[Ir_{13.55}P_9]$ polyanion the Ir9 and Ir13 sites (Fig. 4) show lower occupancies of 77 and 78 %, respectively. This is most likely a geometrical constraint of the structure. These two sites have the shortest Ir–P distances of 227 (Ir7–P9) and 229 pm (Ir13–P7) within

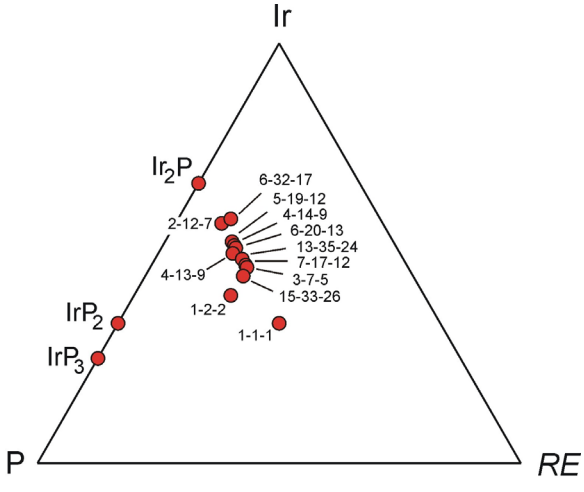

Fig. 6 (color online). Schematic phase diagram for the known $RE_xIr_yP_z$ compositions. Only in this area ternary phosphides are accessible *via* the metal flux technique [10].

the $[Ir_{13.55}P_9]$ polyanion. These two iridium atoms are located at positions where the $ThCr_2Si_2$ slabs of different orientations are *glued* together. Similar iridium defects have been observed for $Lu_3Ir_{6.97}P_5$ [11] and $Sm_{15}Ir_{32.50}P_{26}$ [12].

The iridium substructure of $Ce_4Ir_{13.55}P_9$ is presented in Fig. 5. Except for the *isolated* Ir2 atoms, all iridium atoms are bonded within a three-dimensional framework. The iridium near neighbor coordination of these iridium atoms is interesting. In the lower part of Fig. 5 we present a cutout of the iridium substructure with a view perpendicular to the projection direction. Within the slightly distorted square network we observe a broad range of Ir–Ir distances from 278 to 298 pm. In view of the elemental *fcc* structure of iridium, this near neighbor coordination is peculiar, but also observed for other $RE_xT_yP_z$ phosphides [8]. In typical carbonyl cluster compounds like $[Ir_{11}(CO)_{23}]^{3-}$ (269 – 299 pm Ir–Ir) [28] or $[HIr_5(CO)_{12}]^{2-}$ (260 – 289 pm Ir–Ir) [29] the iridium skeletons resemble the close-packed structures. In the ternary phosphides the strong Ir–P bonding enables formation of the square nets.

Summing up, $Ce_4Ir_{13.55}P_9$ is a new member of the large family of metal-rich phosphides with a metal : phosphorus ratio of 2 : 1. Fig. 6 summarizes the known compositions for the respective $RE_xIr_yP_z$ phosphides. They are all very close in their stoichiometry. Compared to much simpler structure types, the metal-rich $RE_xIr_yP_z$ phosphides show stability ranges for only few rare earth elements, since small changes in the rare earth size (lanthanoid contraction) strongly influence the $[Ir_yP_z]$ networks. More detailed phase analytical studies on these iridium-rich phosphides are going on in order to systematize the stability ranges and structure types.

Acknowledgement

This work was financially supported by the Deutsche Forschungsgemeinschaft.

[1] Yu. Kuz'ma, S. Chykhrij in *Handbook on the Physics and Chemistry of Rare Earths*, Vol. 23, (Eds.: K. A. Gschneidner Jr., L. Eyring), Elsevier Science, Amsterdam, **1996**, chapter 156, pp. 285 – 433.
[2] J. Y. Pivan, R. Guérin, *J. Solid State Chem.* **1998**, *135*, 218.
[3] S. I. Chykhrij, *Pol. J. Chem.* **1999**, *73*, 1595.
[4] C. Le Sénéchal, V. S. Babizhetsky, S. Députier, J. -Y. Pivan, R. Guérin, *Z. Anorg. Allg. Chem.* **2001**, *627*, 1325.
[5] R. Pöttgen, W. Hönle, H. G. von Schnering in *Encyclopedia of Inorganic Chemistry*, 2nd ed., Vol. VII, (Ed.: R. B. King), Wiley, New York, **2005**, pp. 4255-4308.
[6] W. Jeitschko, U. Jakubowski-Ripke, *J. Less-Common Met.* **1985**, *110*, 339.
[7] W. Jeitschko, E. J. Reinbold, *Z. Naturforsch.* **1985**, *40b*, 900.
[8] J. H. Albering, W. Jeitschko, *J. Alloys Compd.* **1996**, *241*, 44.
[9] T. Ebel, J. H. Albering, W. Jeitschko, *J. Alloys Compd.* **1998**, *266*, 71.
[10] M. G. Kanatzidis, R. Pöttgen, W. Jeitschko, *Angew. Chem.* **2005**, *117*, 7156; *Angew. Chem. Int. Ed.* **2005**, *44*, 6996.
[11] U. Pfannenschmidt, U. Ch. Rodewald, R. Pöttgen, *Z. Anorg. Allg. Chem.* **2010**, *636*, 314.
[12] U. Pfannenschmidt, U. Ch. Rodewald, R. Pöttgen, *Z. Kristallogr.* **2010**, *225*, 280.
[13] U. Pfannenschmidt, U. Ch. Rodewald, R. Pöttgen, unpublished results.
[14] K. Yvon, W. Jeitschko, E. Parthé, *J. Appl. Crystallogr.* **1977**, *10*, 73.
[15] G. M. Sheldrick, SHELXS-97, Program for the Solution of Crystal Structures, University of Göttingen, Göttingen (Germany) **1997**. See also: G. M. Sheldrick, *Acta Crystallogr.* **1990**, *A46*, 467
[16] G. M. Sheldrick, SHELXL-97, Program for the Refinement of Crystal Structures, University of Göttingen, Göttingen (Germany) **1997**. See also: G. M. Sheldrick, *Acta Crystallogr.* **2008**, *A64*, 112.
[17] V. Ghetta, P. Chaudouet, R. Madar, J. P. Sénateur, B. Lambert Andron, *Mater. Res. Bull.* **1987**, *22*, 483.
[18] E. Ganglberger, *Monatsh. Chem.* **1968**, *99*, 566.
[19] E. Parthé, B. Chabot, K. Cenzual, *Chimia* **1985**, *39*, 164.
[20] U. Pfannenschmidt, H. Lincke, R. Pöttgen, unpublished results.
[21] A. Löhken, G. J. Reiß, D. Johrendt, A. Mewis, *Z. Anorg. Allg. Chem.* **2005**, *631*, 1144.
[22] J. Emsley, *The Elements*, Oxford University Press, Oxford **1999**.
[23] A. Wurth, A. Löhken, A. Mewis, *Z. Anorg. Allg. Chem.* **2002**, *628*, 661.
[24] A. Löhken, A. Imre, A. Mewis, *Z. Anorg. Allg. Chem.* **2007**, *633*, 137.
[25] G. L. Olcese, G. B. Bonino, *Atti Accad. Naz. Lincei Mat. Nat. Rend.* **1966**, *40*, 629.
[26] J. Donohue, *The Structures of the Elements,* Wiley, New York, **1974**.
[27] H. H. Hill in *Plutonium and other Actinides*, (Ed.: W. N. Mines), Nuclear Materials Series, AIME, Vol. 17, **1970**, p. 2.
[28] R. Della Pergola, L. Garlaschelli, M. Manassero, M. Sansoni, *J. Cluster Sci.* **1999**, *10*, 109.
[29] R. Della Pergola, L. Garlaschelli, M. Manassero, M. Sansoni, D. Strumolo, *J. Cluster Sci.* **2001**, *12*, 23.